Sensors and Materials, Vol. 28, No. 5 (2016) 561–567
MYU Tokyo

S & M 1209

Electrode Spacing Effect on Ultraviolet Photoconductivity of Metal-Semiconductor-Metal Detectors with ZnO Nanorod Arrays Grown by Hydrothermal Method

Chih-Ming Lin, Yi-Cheng Hsu,[1] Shang-Chao Hung,[2*] and Yin-Ming Li[3]

Department of Applied Science, National Taitung University, Taitung 950, Taiwan
[1]Department of Biometranics Engineering, National Pingtung University of Science and Technology, Pingtung 912, Taiwan
[2]Department of Information Technology and Communication, Shih Chien University, Kaohsiung Campus, No. 200, University RD. Neimen, Kaohsiung 845, Taiwan
[3]Institute of Photonics and Communications, National Kaohsiung University of Applied Sciences, Kaohsiung 807, Taiwan

(Received August 31, 2015; accepted January 12, 2016)

Keywords: ZnO, hydrothermal method, photodetectors

In this work, ZnO nanorod (NR) arrays were grown by a hydrothermal method on a ZnO seed-layer-precoated Si (100) substrate. The average diameter and length of the obtained ZnO NRs with a high aspect ratio of 33 are 50 nm and 1.65 μm, respectively. Ultraviolet (UV) metal-semiconductor-metal photodetectors (PDs) were fabricated by plating Au interdigitated electrodes with finger spacings of 100 and 200 μm on the ZnO NR arrays. Illumination and electrode areas were half of the same work area for the two PDs. All measured current-to-voltage curves under UV illumination at 380 nm and in the dark show ohmic contact nature at the interface between Au metal and ZnO NR arrays. Here, the PD with 100 μm finger spacing presented a high photo-to-dark current ratio of 258.2 at 1.0 V bias, and its optical responsivity at 380 nm was about two orders of magnitude larger than that at 450 nm with bias ranging from 0.1 to 5.0 V.

1. Introduction

One-dimensional (1D) semiconductor materials with high surface-to-volume ratio have attracted considerable attention in recent years. Among various 1D semiconductor materials, ZnO nanorods (NRs) have been extensively studied. ZnO is an n-type group II–VI semiconductor material with a large exciton binding energy of 60 meV and a wide-bandgap energy of 3.37 eV at room temperature. ZnO nanostructures exhibit many interesting properties including high photoconductive gain and piezoelectric and photochemical effects,[1–3] and have been widely used in photovoltaic components such as photosensors, light-emitting diodes, gas sensors, and solar cells.[4–10] Recently, much progress has been made in the synthesis of well-aligned 1D ZnO micro- or nanostructures by technologies such as magnetron sputtering, molecular beam epitaxy, chemical vapor deposition, pulsed laser deposition, a hydrothermal method, and a sol–gel process.[11–20] Among them, the hydrothermal method takes the advantages of simplicity, low cost, low growth temperature, and

*Corresponding author: e-mail: schung99@gmail.com

ISSN 0914-4935

easy coating on large substrates.[21] Some investigations have shown the practical applications of photodetectors (PDs) with the ZnO NR arrays fabricated by the hydrothermal method.[22,23]

In this study, ZnO NR arrays on a ZnO-seed-layer-precoated Si (100) substrate were synthesized using precursor solutions of zinc nitrate hexahydrate ($Zn[NO_3]_2 \cdot 6H_2O$) and hexamethylenetetramine ($C_6H_{12}N_4$). The photocurrent, dark current, and responsivity of ultraviolet (UV) PDs based on the ZnO NR arrays, which have Au interdigitated electrodes with spacings of 100 and 200 μm on the top surface of the NRs, were measured and analyzed.

2. Materials and Methods

ZnO NR arrays were synthesized on a Si (100) substrate precoated with a ZnO seed layer by a hydrothermal method. Before the coating of the ZnO seed layer, the substrate was cleaned with alternate acetone and methanol. Then, the substrate was immersed in deionized (DI) water for several minutes and dried in nitrogen gas. The coating solution of zinc acetate [$Zn(CH_3COO_2) \cdot 2H_2O$] dissolved in ethanol ($C_2H_5OH$) was dropped to the cleaned substrate set on a disk of a spincoater with a rotation speed of 2000 rpm for 30 s in air. The spincoating process was repeated 15 times and followed by the anealing of the coated substrate in a furnace to remove water and organic contaminants. Finally, ZnO NR arrays were synthesized on the Si (100) substrate precoated with a ZnO seed layer in an equimolar (0.1 M each) aqueous solution of $Zn[NO_3]_2 \cdot 6H_2O$ (98%) and $C_6H_{12}N_4$ (99.5%) in glass beakers. This process was performed at 95 °C for 2 h for the ZnO-seed-layer-precoated substrate, which was immersed in solution and inclined at 45° in the vertical direction, and then cooled down to room temperature. The substrate with the ZnO NR arrays removed from the solution was rinsed in distilled water and dried overnight. The equipment arrangement for the hydrothermal method is depicted in Fig. 1(a). The surface morphology of the samples with the ZnO NR arrays was characterized using a Hitachi S-4700I field-emission scanning electron microscope (FESEM) operated at 15 kV. The crystal structure and crystallographic orientation of ZnO NR arrays on the Si (100) substrate were investigated using a Siemens D5000 X-ray diffraction (XRD) system. Photoluminescence (PL) measurement was performed using a continuous wave (CW) He–Cd laser operated at 325 nm as an excitation source. A 100-nm-

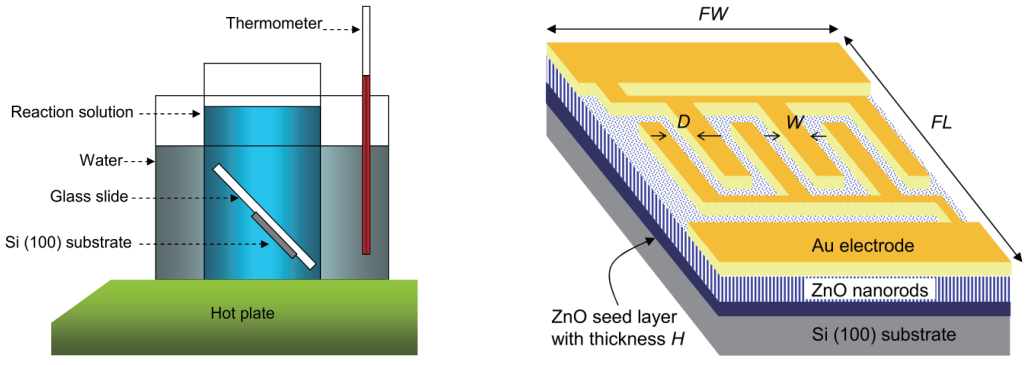

(a) (b)

Fig. 1. (Color online) Schematic diagrams of (a) experimental setup for hydrothermal method and (b) the fabricated photoconductive UV PD based on ZnO NR arrays.

thick Au film was finally plated through an interdigitated shadow mask on the ZnO NR arrays to serve as contact electrodes for fabricating the UV PDs. Figure 1(b) shows a schematic diagram of the fabricated ZnO NR array-based UV PD. The full width (*FW*) and length (*FL*) of the work area of two interdigitated electrodes with finger spacings *D* of 100 and 200 μm are 1950 and 4000 μm, respectively. The entire illumination and electrode areas of the PDs are about $FW \times FL/2$ for different spacings, because the finger electrodes are designed such that the width *W* of the respective finger elements is equal to the spacing *D* between finger elements. The finger coupling number n_c can be approximately calculated as $FW/2(W + D)$ or $FW/4D$ if $W = D$. Current-to-voltage (*I–V*) characteristics of the ZnO NR array-based UV PDs were then measured under illumination and in the dark using a Keithley 2400 digital sourcemeter.

3. Results

Figures 2(a) and 2(b) show the cross-sectional and top-view FESEM images of the ZnO NR arrays, respectively, and display vertically orientated NRs covered the entire substrate with very high area density. The aligned ZnO NRs grow from a ZnO seed layer with a thickness *H* of about 0.4 μm as marked by a couple of arrows in Fig. 2(a). The average diameter and length of the ZnO NRs are about 50 nm and 1.65 μm, respectively. Figure 3 shows the XRD spectrum measured from the ZnO NR arrays grown on the ZnO-seed-layer-precoated Si (100) substrate. A sharp ZnO (002) XRD peak is observed at $2\theta = 34.5°$ and shows that the ZnO NRs have a good crystalline wurtzite structure and a preferred (002) orientation vertical to the surface of the Si (100) substrate. Relatively weak peaks from other ZnO crystallographic plane orientations of (100), (101), (102), (103), and Si (400) were also found. In Fig. 4, the PL spectrum of the ZnO NR arrays measured at room temperature shows a strong UV emission band at 388 nm (3.19 eV) with a full width at half maximum (FWHM) of 162 meV, which corresponds to the recombination of free excitons in ZnO materials. An additional weak green emission band at 538 nm (2.30 eV) corresponding to the interstitial oxygen level is also observed.[24–26]

The UV PDs having Au/ZnO/Au metal-semiconductor-metal structures with Au interdigitated electrodes simply patterned on the top of ZnO NR arrays were then evaluated. The *I–V* characteristics of these PDs measured under UV illumination at 380 nm and in the dark are shown

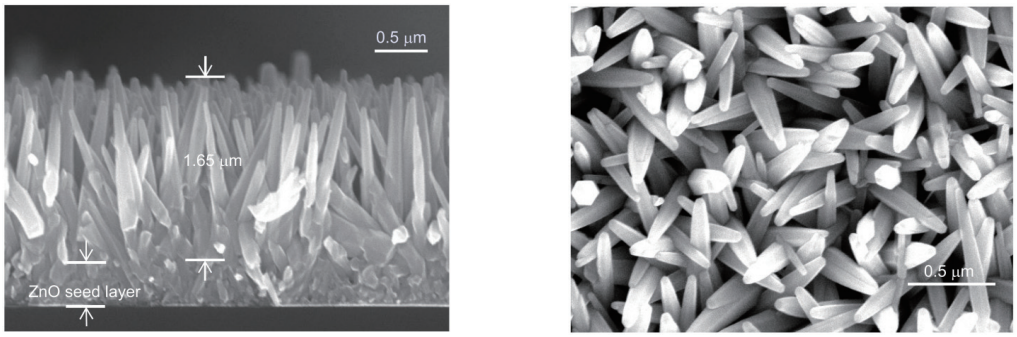

(a) (b)

Fig. 2. (a) Cross-sectional and (b) high-magnification top-view FESEM images of ZnO NR arrays grown on Si (100) substrate.

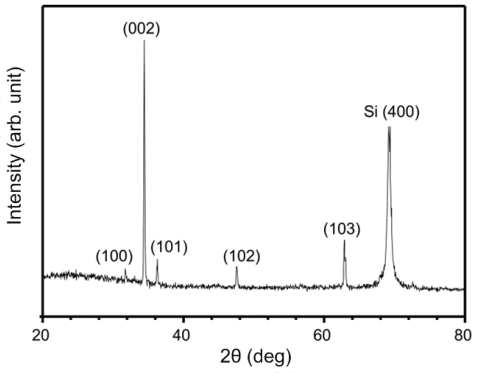

Fig. 3. XRD spectrum measured from the ZnO NR arrays on ZnO-seed-layer-precoated Si (100) substrate.

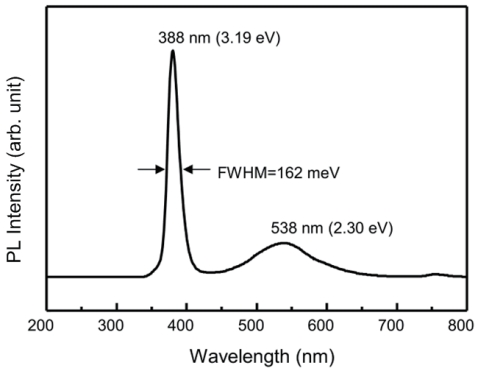

Fig. 4. PL spectrum of the ZnO NRs at room temperature.

in Figs. 5(a) and 5(b), respectively. All currents increase almost linearly with voltages, showing that the interface between the Au film and the ZnO NRs should be treated as an ohmic contact. This ohmic behavior can be explained by an increase in carrier concentration at the interface due to a high donor concentration contributed by oxygen vacancies in ZnO NRs, which leads to a low contact resistivity by increasing the electron tunneling probability through a narrow interface barrier. The PDs exhibit the characteristics of photoconductive sensors. In the photoconductive mode, the charge transport inside the ZnO seed layer is mainly related to the drift of free carriers. The photocurrent and dark current significantly depend on the carrier concentrations generated by photo- and thermal excitations, respectively. The dark current could also be affected by self-heating, which further enhances the carrier concentration in semiconductors. Under illumination on the PDs, most of the free carriers either from ZnO band-to-band excitations or release of electrons by the desorption of oxygen on the surface of the ZnO NRs will concentrate in the NRs, then diffuse downward to the ZnO seed layer, and drift in the ZnO seed layer to reach the electrodes. Photo- and thermally generated carrier concentrations in the ZnO seed layer can be assumed to be equal under different bias conditions for the two PDs. The only difference between the PDs is the total electrode length L_{tot}, which can be expressed by $n_c \times FL$, if $FL >> D$ and W.

4. Discussion

For isothermal assumption, the photocurrent or dark current will monotonically decrease with increasing spacing D because the corresponding conduction cross-sectional area A_{cond} ($= H \times L_{tot}$) of the ZnO seed layer decreases as the currents flow through this layer, and the current density in the ZnO seed layer only depends on carrier generation mechanisms. In Fig. 5(a), the PD with 100 mm spacing has about 1.7-fold larger photocurrents than that with 200 mm spacing, since its length is twofold larger than the total electrode length L_{tot}, and the carrier concentrations generated by photoexcitation are assumed to be close to each other. However, in Fig. 5(b) the dark current increases with the spacing, because the current density is dominated by the concentration of thermally generated carriers, which is much lower than that of photogenerated carriers and could be affected by the self-heating effect. The PD with larger spacing D and smaller conduction cross-

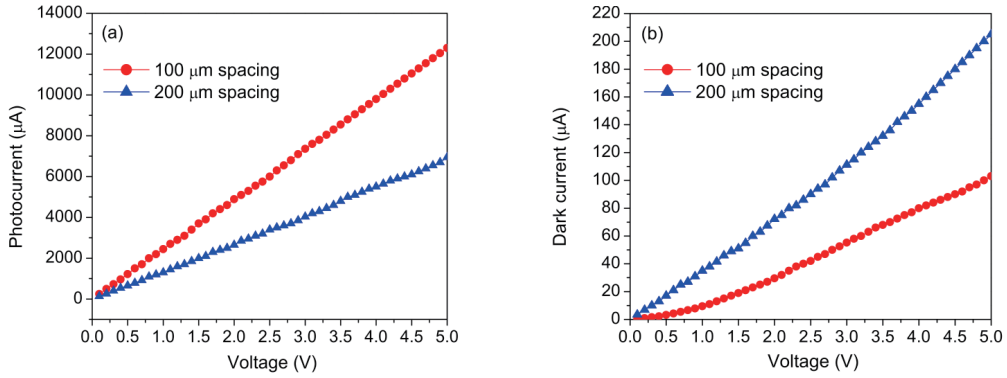

(a) (b)

Fig. 5. (Color online) *I–V* characteristics of the ZnO NR array-based photoconductive UV PDs with finger spacings of 100 and 200 μm measured (a) under UV illumination at 380 nm and (b) in the dark.

Table 1
Photocurrents, dark currents, and photo-to-dark current ratios of the photoconductive UV PDs for different finger spacings and applied biases.

	100 μm spacing			200 μm spacing		
Bias (V)	I_{photo} (μA)	I_{dark} (μA)	I_{photo}/I_{dark}	I_{photo} (μA)	I_{dark} (μA)	I_{photo}/I_{dark}
0.1	243.7	0.4	641.3	142.2	3.4	41.8
0.5	1219.4	3.2	383.5	722.3	17.1	42.2
1.0	2443.0	9.5	258.2	1453.3	34.8	41.8
2.0	4893.2	29.5	165.9	2926.3	72.2	40.6
3.0	7356.2	55.3	133.0	4350.5	111.2	38.7
4.0	9800.5	80.0	122.5	5500.0	155.0	35.5
5.0	12300.2	103.1	119.3	6950.3	205.3	33.9

sectional area A_{cond} will have a higher equilibrium working temperature due to a larger resultant resistance in the ZnO seed layer, which induces more thermal generated carriers to increase the carrier concentration, and thus have larger dark currents. Here, the heat dissipation rate is assumed to be the same for the two PDs with equal illumination and electrode areas, if most heat is transferred by conduction via the large surface area of the ZnO NR arrays.

In the hydrothermal growing method, the higher concentration of precursor solution induces a much larger crystal nucleus, which results in the increased dimensions of NRs and the change in the characteristics of the ZnO NRs. The solution temperature was set at 95 °C during the hydrothermal process to completely synthesize the ZnO NRs without boiling water. The higher solution temperature induces the faster growth, which results in the increased numbers of dislocations and defects and even branch structures. Moreover, the aspect ratio of the NRs is reduced. The temperature effect during the hydrothermal process and postannealing of the ZnO NRs are worth to investigate more details in the future.

As shown in Table 1, the ZnO NR array-based photoconductive UV PD with 100 μm finger spacing, which has a relatively high signal-to-noise ratio (I_{photo}/I_{dark}), was used to evaluate its optical responsivity in detail. Figure 6 shows the spectral responsivities of this PD at the bias from 0.1 to 5.0 V and the illumination wavelength from 300 to 500 nm. The cutoff points all appeared at 380 nm,

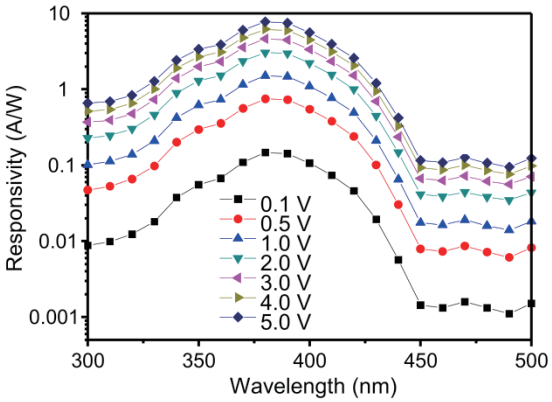

Fig. 6. (Color online) Spectral responsivity measurements of the ZnO NR array-based photoconductive UV PD with a finger spacing of 100 μm.

and the responsivity at 1.0 V bias was 1.46 A/W. Because the responsivities of the PD at 380 nm are about two orders of magnitude larger than those at 450 nm under different biases, the PD could be used as a good visible-blind UV PD.

5. Conclusions

We demonstrated photoconductive UV PDs based on the photoabsorption layer of ZnO NR arrays, which were fabricated by a hydrothermal method on a ZnO-seed layer-precoated Si (100) substrate. The diameter and length of ZnO NRs are about 50 nm and 1.65 μm, respectively, and a high aspect ratio of 33 can be obtained. For easier processing, a Au film was finally plated on the PDs to serve as interdigitated electrodes on top of the ZnO NRs. Linear $I-V$ curves under UV illumination at 380 nm and in the dark show that the interface between the Au film and the ZnO NRs should be treated as an ohmic contact. When the illumination area is equal to the electrode area for interdigitated electrodes, the PD with a wider finger spacing has a larger dark current, because the corresponding concentration of thermally generated carriers becomes higher with the self-heating effect due to a larger resultant resistance in the conduction path through the ZnO seed layer. The photoconductive UV PD with a finger spacing of 100 μm has cutoff points all appearing at 380 nm, and its optical responsivities at 380 nm are about two orders of magnitude larger than those at 450 nm under different biases. It has I_{photo}= 2443.0 μA, I_{dark}= 9.5 μA, I_{photo}/I_{dark}= 258.2, and responsivity = 1.46 A/W at 1.0 V bias and 380 nm illumination wavelength. This article shows that the photoconductive UV PD based on ZnO NR arrays with an appropriate electrode spacing can exhibit high signal-to-noise and UV-to-visible rejection ratios, and may become potentially useful for practical applications of visible-blind UV PDs.

Acknowledgements

This work was supported by the Ministry of Science and Technology under the contract number MOST-104-2221-E-158-003 and the Shih Chien University, Kaohsiung Campus, under the contract number USC-104-05-05008.

References

1 T. P. Chen, S. J. Young, S. J. Chang, and C. H. Hsiao: IEEE Sens. J. **11** (2011) 3457.
2 J. H. Lee, K. Y. Lee, B. Kumar, and S. W. Kim: J. Nanosci. Nanotechnol. **12** (2012) 3430.
3 I. Bedja: Adv. Optoelectron. **2011** (2011) 1.
4 N. Liu, G. Fang, W. Zeng, H. Zhou, F. Cheng, Q. Zheng, L. Yuan, X. Zou, and X. Zhao: ACS Appl. Mater. Interfaces **2** (2010) 1973.
5 L. Wang, D. Zhao, Z. Su, F. Fang, B. Li, Z. Zhang, D. Shen, and X. Wang: Org. Electron. **11** (2010) 1318.
6 H. K. Lee, M. S. Kim, and J. S. Yu: IEEE Photonic. Tech. L. **23** (2011) 1204.
7 J. Xu, Y. Chen, D. Chen, and J. Shen: Sens. Actuators, B **113** (2006) 526.
8 C. Cheng, G. Xu, H. Zhang, and Y. Luo, J. Nanosci. Nanotechnol. **7** (2007) 4439.
9 J. Chung, J. Lee, and S. Lim: Phys. Rev. B **405** (2010) 2593.
10 Y. H. Ko and J. S. Yu: J. Nanosci. Nanotechnol. **10** (2010) 8095.
11 I. J. Kim, I. S. Kim, S. K. Kim, and S. Y. Choi: Jpn. J. Appl. Phys. **48** (2009) 08HJ03.
12 K. Ogata, K. Koike, S. Sasa, M. Inoue, and M. Yano: Semicond. Sci. Tech. **24** (2009) 015006.
13 L. C. Tien, D. P. Norton, S. J. Pearton, H. T. Wang, and F. Ren: Appl. Surf. Sci. **253** (2007) 4620.
14 B. Tang, H. Deng, Z. W. Shui, and Q. Zhang: J. Nanosci. Nanotechnol. **10** (2010) 1842.
15 K. Kitamura, T. Yatsui, M. Ohtsu, and G. C. Yi: Nanotechnology **19** (2008) 175305.
16 C. V. Varanasi, K. D. Leedy, D. H. Tomich, G. Subramanyam, and D. C. Look: Nanotechnology **20** (2009) 385706.
17 H. Ghayour, H. R. Rezaie, S. Mirdamadi, and A. A. Nourbakhsh: Vacuum **86** (2011) 101.
18 S. F. Wang, T. Y. Tseng, Y. R. Wang, C. Y. Wang, and H. C. Lu: Ceram. Int. **35** (2009) 1255.
19 S. Amizam, M. H. Mamat, Z. Khusaimi, H. A. Rafaie, M. Z. Sahdan, S. Abdullah, and M. Rusop: Mater. Res. Innov. **13** (2009) 189.
20 Y. Lin, D. Wang, Q. Zhao, Z. Li, Y. Ma, and M. Yang: Nanotechnology **17** (2006) 2110.
21 B. Liu and H. C. Zeng: J. Am. Chem. Soc. **125** (2003) 4430.
22 H. H. Huang, G. J. Fang, X. M. Mo, L. Y. Yuan, H. Zhou, M. J. Wang, H. B. Xiao, and X. Z. Zhao: Appl. Phys. Lett. **94** (2009) 063512.
23 T. P. Chen, S. J. Young, S. J. Chang, C. H. Hsiao, and Y. J. Hsu: Nanoscale Res. Lett. **7** (2012) 214.
24 W. D. Yu, X. M. Li, and X. D. Gao: Appl. Phys. Lett. **84** (2004) 2658.
25 A. F. Aktaruzzaman, G. L. Sharma, and L. K. Malhotra: Thin Solid Films **198** (1991) 67.
26 F. Li, Z. Li, and F. J. Jin: Mater. Lett. **61** (2007) 1876.